How to cite: *Angew. Chem. Int. Ed.* **2022,** *61,* e202205914
International Edition: doi.org/10.1002/anie.202205914
German Edition: doi.org/10.1002/ange.202205914

Supramolecular Chemistry

Spontaneous Resolution of Helical Building Blocks through the Formation of Homochiral Helices in Two Dimensions

Xiang Lin, Bohan Kou, Jinlian Cao, Peimin Weng, Xiaosheng Yan, Zhao Li,* and Yun-Bao Jiang**

Abstract: Spontaneous resolution leading to conglomerate crystals remains a significant challenge. Here we propose the formation of orthogonal homochiral supramolecular helices in at least two dimensions to allow spontaneous resolution. We suggest the design rationale that the chiral species is made into helical building blocks to allow the helix formation. As a proof-of-concept, acetylalanine was made into a helical short azapeptide, its *N*-amidothiourea derivative containing a β-turn structure, to which a halogen atom was further introduced at the phenylthiourea aromatic ring. The resultant folded species undergoes both intermolecular hydrogen and halogen bonding across the turn structure to form orthogonal intermolecular hydrogen-bonded and halogen-bonded supramolecular helices in two dimensions, and undergoes chiral resolution upon crystallization. Meanwhile, counterparts containing either an F-substituent with weak halogen bonding or no halogen atom crystallize as racemic compounds.

Introduction

The rational design of molecules undergoing spontaneous resolution in conglomerate crystals remains a challenge. Only approximately 5–10 % of the racemates crystallize in the form of a conglomerate, a mechanical mixture of crystals of the two pure enantiomers, whereas over 90 % of them crystallize as racemic compounds in which two enantiomers co-exist in a single crystalline phase in a molar ratio of 1 : 1.[1] It remains hard to predict whether crystals will be conglomerate:[2,3] too many thermodynamic and kinetic factors are involved in the processes of crystal nucleation and growth.[4–6]

[*] X. Lin, B. Kou, Dr. J. Cao, P. Weng, Dr. X. Yan, Dr. Z. Li, Prof. Dr. Y.-B. Jiang
Department of Chemistry, College of Chemistry and Chemical Engineering, The MOE Key Laboratory of Spectrochemical Analysis and Instrumentation, and iChEM, Xiamen University
Xiamen 361005 (China)
E-mail: xshyan@xmu.edu.cn
lizhao@xmu.edu.cn
ybjiang@xmu.edu.cn
Dr. X. Yan
School of Pharmaceutical Sciences, Xiamen University
Xiamen 361102 (China)

Note that the formation of conglomerates means that enantiomers of the same chirality crystallize together, a kind of homochirality occurring during the crystallization. This is reminiscent of the observation made for a supramolecular helix consisting mainly of homochiral building blocks,[7–9] a consequence of the homochiral elongation along the axis of the one-dimensional (1D) helix.[10] Indeed, supramolecular helices were observed in many conglomerate crystals,[11–20] yet the formation of a 1D helix does not necessarily ensure the formation of a conglomerate crystal from enantiomers,[21] because the formation of a conglomerate crystal requires homochiral elongation along three different crystallographic axes. This means making the enantiomers form supramolecular helices along two or more crystallographic axes (in two or more dimensions), which would allow the formation of a homochiral three-dimensional (3D) crystal, could be a means to spontaneous resolution. We recently showed that a short peptide that was converted into its amidothiourea derivative folds because of the β-turn structure maintained by a ten-membered ring intramolecular hydrogen bond.[22–25] When an additional interaction such as halogen bonding is introduced, the folded helical building block may assemble, via halogen bonding and hydrogen bonding, into supramolecular helices, allowing likely spontaneous resolution. As a proof-of-concept, we report here how we modified acetylalanine as its *N*-amidothiourea derivative, which was further equipped with a halogen atom of sufficiently strong halogen-bonding ability, such as I, Br, or Cl (Scheme 1a) and underwent self-assembly to form supramolecular helices. Here, spontaneous resolution does occur as a result of the formation of orthogonal supramolecular helices in two dimensions (Scheme 1b). Derivatives in which X = F or H are unable to undergo intermolecular halogen bonding, despite hydrogen bonding, and they crystallize as racemic compounds.

Results and Discussion

We recently showed that bilateral *N*-amidothioureas containing I substituents at two terminal phenyl rings formed 1D supramolecular helices with homochiral preference, in which the propagation of the helicity of the helical β-turn structure along the helix was assumed responsible.[26–29] We thus envisaged that if we cut the bilateral compound in half, the original propagation pathway would be blocked, and that if the interaction elements remain, other propagation pathways would be established during the assembly via

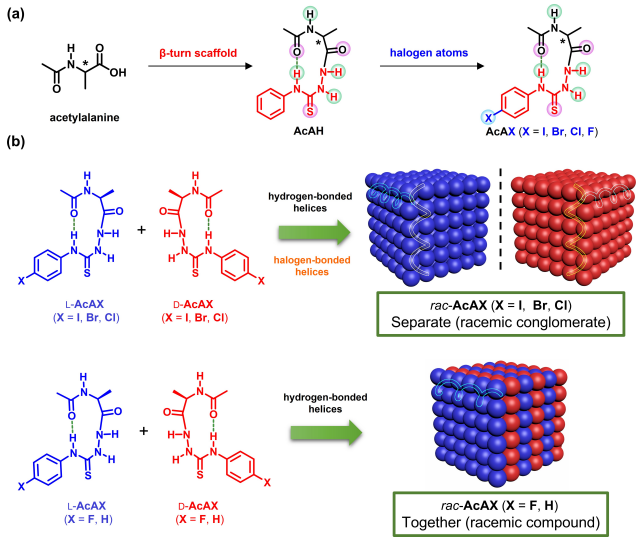

Scheme 1. a) Chemical structures of acetylalanine, *N*-amidothiourea **AcAH**, and its halogenated counterparts **AcAI**, **AcABr**, **AcACl**, and **AcAF**. The green and blue balls indicate potential donors in intermolecular hydrogen and halogen bonding, respectively, while purple balls highlight potential acceptors in intermolecular hydrogen and halogen bonding. b) Schematic representation of racemic conglomerates for *rac*-**AcAI**, *rac*-**AcABr**, and *rac*-**AcACl** crystals, and racemic compounds for *rac*-**AcAF** and *rac*-**AcAH** crystals. All crystals contain a β-turn structure. Green dashed lines highlight intramolecular hydrogen bonds for the β-turn structure.

interactions across the turn structure. We thus came to our model compound to test our hypothesis for spontaneous resolution, the acetylalanine-based *N*-amido-*N*′-phenyl-thiourea containing a halogen atom at the *para* position of the *N*′-phenyl ring (Scheme 1). In these compounds there are two kinds of intermolecular interactions across the turn structure, i.e. amide–amide type hydrogen bonding and C–X···S halogen bonding, which may lead to two kinds of supramolecular helices and eventually lead to spontaneous resolution.

Absorption and circular dichroism (CD) spectra of L-**AcAX** (**X**=**I**, **Br**, **Cl**, **F**, **H**[23]) measured in CH_3CN (Figure S1) confirm the existence of the β-turn structure. Crystals of enantiomers and racemates of **AcAX** (**X**=**I**, **Br**, **Cl**, **F**, **H**) were successfully grown, by slow evaporation of their 1:1 (v/v) CH_3CN/CH_3OH solutions and subjected to X-ray crystallography for structural characterization (for detailed crystallographic data, see Tables S1–S5). First we examined the crystal structures of enantiopure and racemic **AcAI**, in which the I substituent could provide the strongest halogen bonding. *rac*-**AcAI** crystallizes as a conglomerate, with a chiral space group of $P2_12_12_1$. Of seven crystals in one pot, four are enantiopure L-**AcAI** crystals and three are enantiopure D-**AcAI** crystals, following individual single-crystal structural analysis (Table S6). CD spectra and chiral high-performance liquid chromatography (HPLC) traces of selected single *rac*-**AcAI** crystals show that they are either pure L-**AcAI** or pure D-**AcAI** crystals (Figure 1a and b), confirming the nature of the conglomerates of the crystallized *rac*-**AcAI**. Accordingly, the X-ray powder diffraction (XRPD) pattern of the *rac*-**AcAI** crystal was found to be identical to that of the enantiopure L-**AcAI** crystal (Figure 1c).

To clarify the mechanisms for the formation of conglomerate from *rac*-**AcAI**, the X-ray crystal structure of enantio-

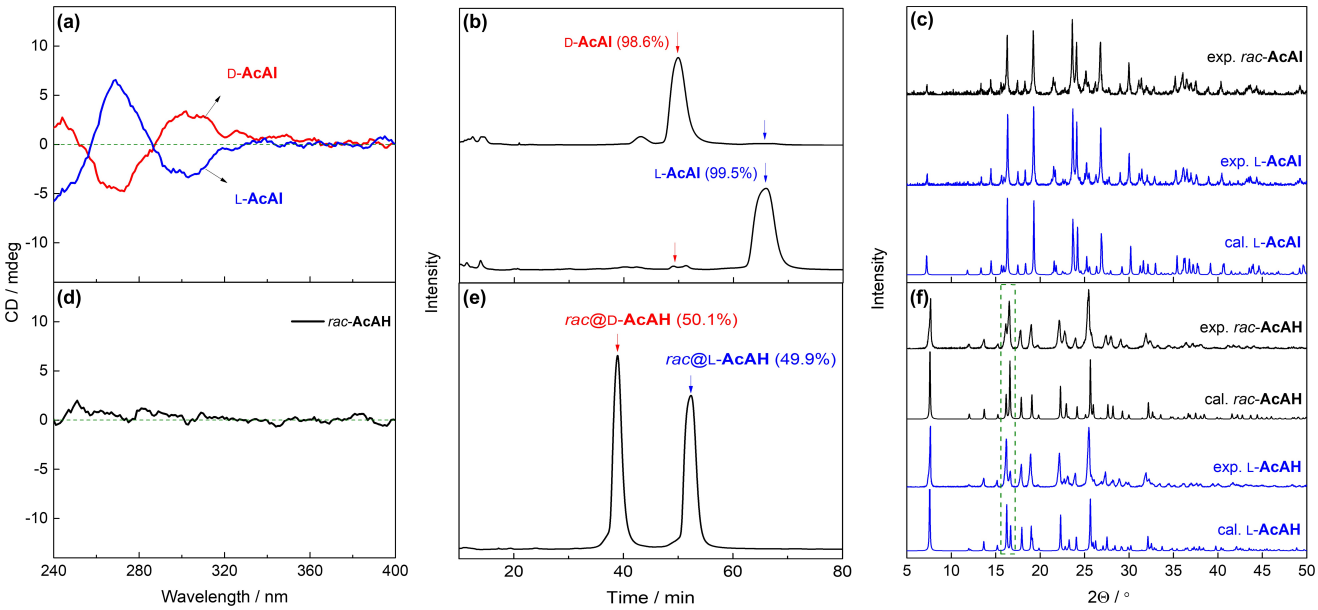

Figure 1. a) CD spectra of selected single *rac*-**AcAI** crystals. b) HPLC traces of selected single *rac*-**AcAI** crystals. c) Calculated and experimental XRPD patterns of L-**AcAI** crystals and experimental XRPD pattern of *rac*-**AcAI** crystals. The results shown in (a, b, c) indicate that *rac*-**AcAI** forms racemic conglomerates. d) CD spectrum of a selected single *rac*-**AcAH** crystal. e) HPLC trace of a selected single *rac*-**AcAH** crystal. f) Calculated and experimental XRPD patterns of L-**AcAH** and *rac*-**AcAH** crystals. The results presented in (d, e, f) indicate that *rac*-**AcAH** forms racemic compounds.

pure L-**AcAI** was next examined. Along the crystallographic *b*-axis, L-**AcAI** molecules containing a βII turn (for parameters of β-turns, see Table S7) interact via the amide–amide like N–H^{c}···^{f}O=C and N–H^{a}···S=C hydrogen bonds across the turn structures, resulting in a supramolecular left-handed (*M*) helix with a pitch of 7.90 Å (Figure 2a, b, d, Table 1). Further N–H^{b}···^{e}O=C hydrogen bonds bridge these *M*-helices parallel along the *a*-axis to form a homochiral two-dimensional (2D) nanostructure (Figure 2c, e). Along the *c*-axis, these homochiral 2D layers stack via the C–I···S halogen bonds, also across the turns, into a 3D-superstructure (Figure 3a). The C–I···S halogen bonding actually leads to a supramolecular *M*-helix of L-**AcAI** along the *a*-axis, with a pitch of 7.86 Å (Table 1). Therefore, the hydrogen bonding and halogen bonding in the crystals of L-**AcAI** lead to supramolecular *M*-helices along *b*- and *a*-axes, respectively (Figures 2d and 3a), generating helices in two dimensions that eventually ensure a global homochiral 3D nanostructure (Figure 3b). In all these helices, a homochiral preference exists, allowing therefore good propagation of the helicity of the β-turn structure. Crystals of D-**AcAI** show superstructures symmetric to those of L-**AcAI**, containing simultaneously the hydrogen-bonded and halogen-bonded right-handed (*P*) helices in two dimensions (Figure S2).

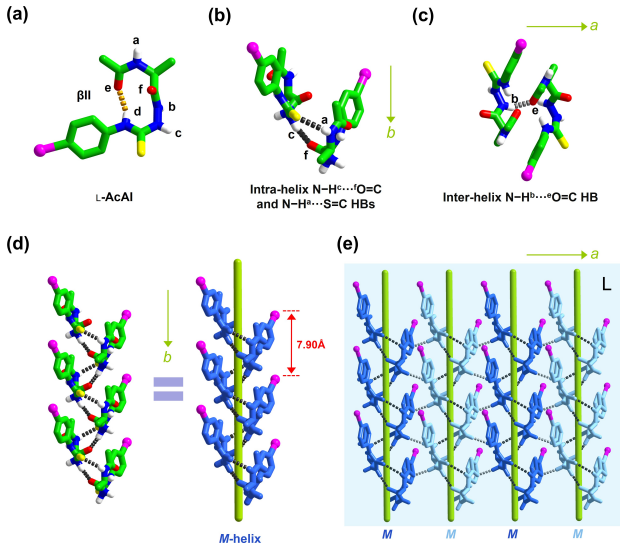

Figure 2. 2D superstructure of L-**AcAI** in its X-ray crystal structure. a) Crystal structure of L-**AcAI** showing a βII turn. b) N–H^{c}···^{f}O=C and N–H^{a}···S=C hydrogen bonds (dashed black lines) within the helix along the *b*-axis. c) N–H^{b}···^{e}O=C hydrogen bond (dashed gray line) along the *a*-axis, between neighboring helices. d) Single-strand *M*-helix from L-**AcAI** molecules along the *b*-axis linked by N–H^{c}···^{f}O=C and N–H^{a}···S=C hydrogen bonds (dashed black lines). e) Supramolecular 2D structure from parallel *M*-helices of L-**AcAI** formed via N–H^{b}···^{e}O=C hydrogen bonds (dashed gray lines) along the *a*-axis, between neighboring helices. For clarity, –CH hydrogens are omitted.

Other derivatives of **AcAI** containing a Br or Cl substituent of strong halogen-bonding ability, **AcABr** or **AcACl** (Scheme 1), were also found to undergo spontaneous resolution, according to the X-ray crystal structural analysis, XRPD patterns, solid CD spectra, and chiral HPLC traces (Figures S3–S10). Again, L-**AcABr** and L-**AcACl** form, like L-**AcAI**, both the hydrogen- and halogen-bonded (C–Br···S or C–Cl···S, Table 1) supramolecular *M*-helices, affording homochiral 3D nanostructures and thereby conglomerate crystals (Figures S3 and S7). The fact that the hydrogen-bonding modes and the structural parameters remain more or less unchanged when the halogen atom is changed from I to Br to Cl (**AcAX**, **X** = **I**, **Br**, **Cl**; Table 1) indicates that the hydrogen bonding and halogen bonding that lead to helices in two dimensions are orthogonal.

However, derivatives **AcAF** and **AcAH** (Scheme 1) containing an F-substituent of weak halogen-bonding ability or no halogen atom, respectively, were found to crystallize as racemic compounds. Crystals of D-**AcAH** show a chiral $P2_12_12_1$ space group like that of L-**AcAH**,[23] whereas crystals of the racemic mixture *rac*-**AcAH** feature an achiral $Pna2_1$ space group (Table 1). The lack of a CD feature for a single *rac*-**AcAH** crystal in its solid-state CD spectrum (Figure 1d),

Table 1: Crystal system, space group and parameters of the hydrogen-/halogen-bonded supramolecular helices from acetyl(L-alanine) based azapeptides in their enantiopure and racemic crystals.

Building block	Crystal system	Space group	Sense	Helical pitch [Å]	Hydrogen/halogen bonding
L-**AcAI**	orthorhombic	$P2_12_12_1$	*M*	7.90	N–H^{c}···^{f}O=C ($d_{H\cdots O}$ = 2.106 Å; ∠NHO = 147.3°) N–H^{a}···S=C ($d_{H\cdots S}$ = 2.720 Å; ∠NHS = 143.0°)
			M	7.86	C–I···S ($d_{I\cdots S}$ = 3.488 Å; ∠CIS = 172.5°)
L-**AcABr**	orthorhombic	$P2_12_12_1$	*M*	7.83	N–H^{c}···^{f}O=C ($d_{H\cdots O}$ = 2.111 Å; ∠NHO = 144.5°) N–H^{a}···S=C ($d_{H\cdots S}$ = 2.716 Å; ∠NHS = 143.6°)
			M	7.86	C–Br···S ($d_{Br\cdots S}$ = 3.483 Å; ∠CBrS = 170.0°)
L-**AcACl**	orthorhombic	$P2_12_12_1$	*M*	7.78	N–H^{c}···^{f}O=C ($d_{H\cdots O}$ = 2.109 Å; ∠NHO = 143.9°) N–H^{a}···S=C ($d_{H\cdots S}$ = 2.711 Å; ∠NHS = 144.1°)
			M	7.87	C–Cl···S ($d_{Cl\cdots S}$ = 3.542 Å; ∠CClS = 168.3°)
L-**AcAF**	monoclinic	*I*2	*M*	7.84	N–H^{c}···^{f}O=C ($d_{H\cdots O}$ = 2.125 Å; ∠NHO = 147.6°) N–H^{a}···S=C ($d_{H\cdots S}$ = 2.691 Å; ∠NHS = 145.3°)
rac@L-**AcAF**	orthorhombic	$Pna2_1$	*M*	7.87	N–H^{c}···^{f}O=C ($d_{H\cdots O}$ = 2.130 Å; ∠NHO = 147.3°) N–H^{a}···S=C ($d_{H\cdots S}$ = 2.721 Å; ∠NHS = 144.3°)
L-**AcAH**	orthorhombic	$P2_12_12_1$	*M*	7.66	N–H^{c}···^{f}O=C ($d_{H\cdots O}$ = 2.137 Å; ∠NHO = 141.9°) N–H^{a}···S=C ($d_{H\cdots S}$ = 2.729 Å; ∠NHS = 145.4°)
rac@L-**AcAH**	orthorhombic	$Pna2_1$	*M*	7.74	N–H^{c}···^{f}O=C ($d_{H\cdots O}$ = 2.104 Å; ∠NHO = 143.4°) N–H^{a}···S=C ($d_{H\cdots S}$ = 2.695 Å; ∠NHS = 144.6°)

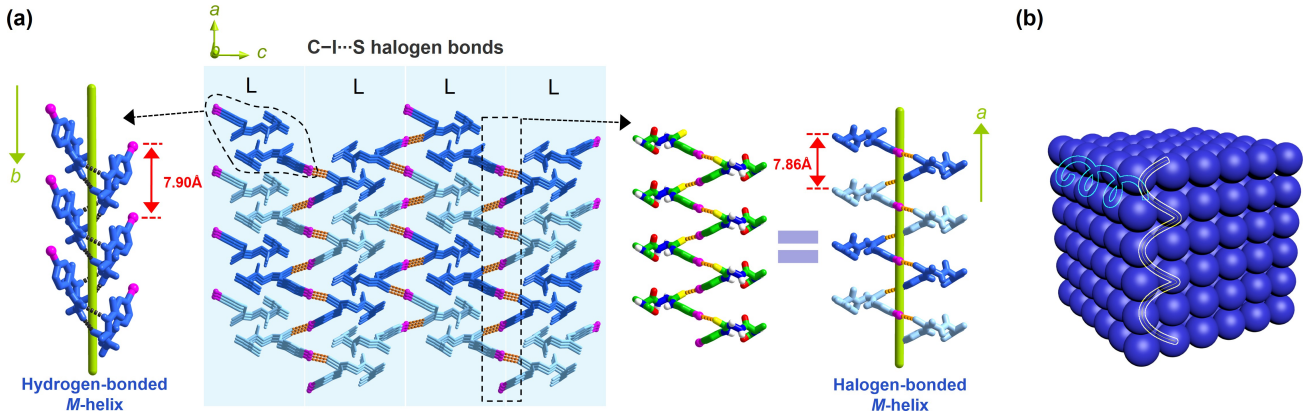

Figure 3. 3D superstructure of L-**AcAI** in its X-ray crystal structure. a) Homochiral 2D layers from hydrogen-bonded *M*-helices of L-**AcAI** are linked by C–I···S halogen bonds along the *c*-axis, leading to a halogen-bonded L-**AcAI** *M*-helix. For clarity, all hydrogens in the 3D structure are omitted. b) Schematic representation of supramolecular helices in two dimensions that afford a global homochiral 3D nanostructure.

equivalent amounts of L-**AcAH** and D-**AcAH** in the HPLC profile of the *rac*-**AcAH** crystal sample (Figure 1e), and the different XRPD patterns of *rac*-**AcAH** and L-**AcAH** crystals (Figure 1f) all support the racemic character of the crystals of *rac*-**AcAH**.

In the *rac*-**AcAH** crystals, L-**AcAH** and D-**AcAH** with mirror-image structures were identified, containing the βII and βII′ turns, respectively (Figures 4a and S11a). However, when we examined L-**AcAH** in the *rac*-**AcAH** crystal (labeled as *rac*@L-**AcAH**), we noted that along the crystallographic *c*-axis, N–H^{c}···^{f}O=C and N–H^{a}···S=C hydrogen bonds bridge homochiral *rac*@L-**AcAH** molecules to form a 1D supramolecular helix of *M*-helicity of a pitch of 7.74 Å (Figure 4b, d, Table 1), which has the same hydrogen bonding modes and helix helicity as the supramolecular helices of L-**AcAI** (Figure 2), again suggesting the orthogonality of the hydrogen and halogen bonding. It is worth noting that in these helices a local homochirality is established, since even in the presence of the other enantiomer, D-**AcAH**, the formed helix consists of only the L-**AcAH** molecules. Along *a*-axis, these parallel *M*-helices from *rac*@L-**AcAH** are linked by N–H^{b}···^{e}O=C hydrogen bonds between neighboring helices, leading to a supramolecular 2D structure of homochirality too (Figure 4c and e), like that observed from L-**AcAI** (Figure 2 and Table 1). Meanwhile, *rac*@D-**AcAH** molecules in the crystals of *rac*-**AcAH** form a homochiral 2D nanostructure consisting of parallel *P*-helices from all of the D-**AcAH** molecules (Figure S11), symmetric to that of *rac*@L-**AcAH**.

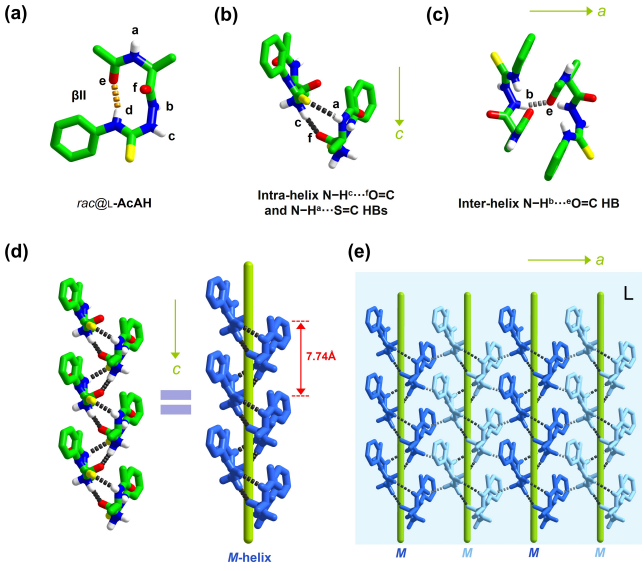

Figure 4. a) Crystal structure of *rac*@L-**AcAH**, showing a βII turn. b) N–H^{c}···^{f}O=C and N–H^{a}···S=C hydrogen bonds (dashed black lines) along the *c*-axis leading to *M*-helix. c) N–H^{b}···^{e}O=C hydrogen bond (dashed gray line) along the *a*-axis, between neighboring helices. d) Single-strand *M*-helix from *rac*@L-**AcAH** molecules along the *c*-axis through N–H^{c}···^{f}O=C and N–H^{a}···S=C hydrogen bonds (dashed black lines). e) Supramolecular 2D structure from parallel *M*-helices of *rac*@L-**AcAH** through N–H^{b}···^{e}O=C hydrogen bonds between neighboring helices (dashed gray lines) along the *a*-axis. For clarity, –CH hydrogens are omitted.

Along the *b*-axis, the homochiral 2D layers, defined by axes *a* and *c* from the parallel *M*-helices of *rac*@L-**AcAH** and *P*-helices of *rac*@D-**AcAH**, respectively, stack alternately via van der Waals interactions, resulting in racemic 3D crystals (Figure 5a). This explains the observation that *rac*-**AcAH** crystallizes as a racemic compound, despite the presence of a local homochiral 2D nanostructure in the formed supramolecular helices in the layers defined by *a*- and *c*-axes.

Crystal structures of enantiomers L-**AcAH** and D-**AcAH** were found to be mirror images (Figures S12 and S13). Homochiral 2D layers consisting of parallel *M*-helices are formed in L-**AcAH** in the same was as those in *rac*@L-**AcAH** (Figures S12 and 4, Table 1), which further stack into a 3D superstructure via van der Waals interactions (Figure 5b). It is significant to observe that the same 1D-helix and homochiral 2D layer are formed from *rac*@L-**AcAH** as those in pure L-**AcAH**, even in the presence of the other enantiomer in the case of racemic **AcAH**. This means that the hydrogen bonding leading to the 1D-helix is orthogonal to other interactions occurring during the crystallization,

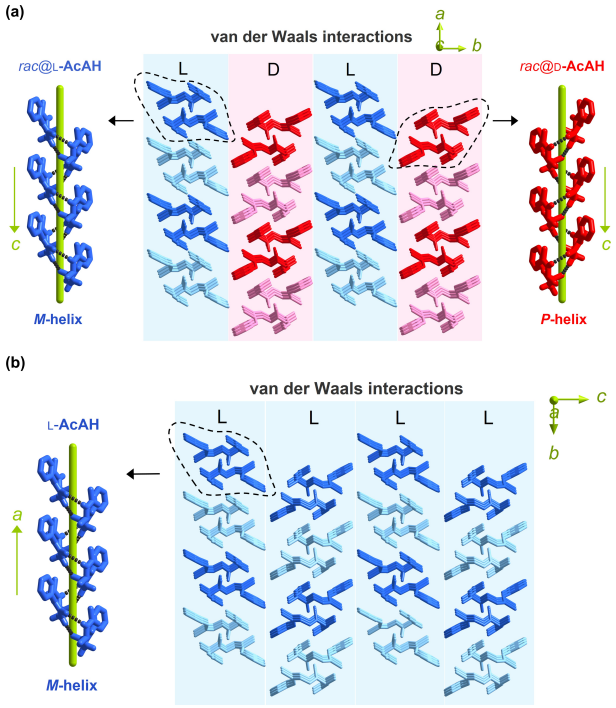

Figure 5. 3D superstructures of *rac*-**AcAH** (a) and L-**AcAH** (b) in their X-ray crystal structures. Homochiral 2D layers of *rac*@L-**AcAH** made up of *M*-helices and those of *rac*@D-**AcAH** made up of *P*-helices are alternately stacked via van der Waals interactions along the *b*-axis, leading to racemic 3D crystals, while homochiral 2D layers of *M*-helices consisting of L-**AcAH** stack in antiparallel manner, also via van der Waals interactions along the *c*-axis, leading to 3D crystals. For clarity, all hydrogens in the 3D structure are omitted. Crystallographic data for L-**AcAH** have previously been reported (CCDC 1820148).[23]

and allows good propagation of the helicity of the β-turn structure along the 1D-helix.

The 3D superstructure in the *rac*-**AcAF** crystal is similar to that of *rac*-**AcAH** (Figure S14 and Figure 5a, Table 1), while XRPD patterns, solid CD spectra, and chiral HPLC traces (Figures S15–S18) indicate that *rac*-**AcAF** crystallizes as a racemic compound.

A significant difference between the superstructures of **AcAF**/**AcAH** and **AcAI**/**AcABr**/**AcACl** is the interactions between 2D layers consisting of parallel helices. In the superstructures of **AcAF**/**AcAH**, it is the non-directional van der Waals interactions that lead to the heterochiral 3D nanostructures; whereas in superstructures of **AcAI**/**AcABr**/**AcACl**, the directional C–X···S (X = I, Br, Cl) halogen bonding leads to a supramolecular helix preferring homochirality, allowing homochiral 3D nanostructures and thereby the spontaneous resolution of *rac*-**AcAI**/**AcABr**/**AcACl**. The occurrence of the halogen bonding in the crystals of **AcAI**/**AcABr**/**AcACl** was further supported by infrared (IR) spectroscopy. Compared to the analogous IR band of L-**AcAF** and L-**AcAH**, the stretching vibration of the C=S double bond in the thiourea moiety of L-**AcAI**, L-**AcABr**, and L-**AcACl** is red-shifted to around 1525 cm^{-1} (Figure S19), in line with the C–X···S (X = I, Br, Cl) halogen bonding in L-**AcAI**, L-**AcABr**, and L-**AcACl** crystals.[30,31] It also deserves pointing out that those crystals can be grown in several other solvents such as CH_3CN, CH_3OH, C_2H_5OH, DMSO, and DMF, and similar observations were made for crystals grown in 1:1 (v/v) CH_3CN/CH_3OH, without inclusion of solvent molecules in the crystals.

Conclusion

In conclusion, we propose and demonstrate that the formation of supramolecular helices in two dimensions leads to spontaneous resolution of the folded short peptides. As an example, acetylalanine was converted into *N*-amidothiourea derivatives with a halogen substituent (I, Br, Cl) at the terminal phenylthiourea ring, to enable intermolecular hydrogen bonding and halogen bonding across the β-turn structure. Supramolecular helices in two dimensions driven by hydrogen bonding and halogen bonding that are orthogonal to each other are formed such that the homochiral 3D nanostructure is ensured. This work thus represents a rational design of molecules undergoing spontaneous resolution in the chiral center in the original chiral compound is included within a helical structure that is constructed to allow intermolecular interactions to form orthogonal helices in at least two dimensions.

Acknowledgements

We acknowledge the support of this work by the NSF of China (Grants 21820102006, 91856118, 21521004, 21435003, and 22101240), the MOE of China (Grant IRT13036), and the scientific and technological project in Xiamen (Grant 3502Z20203025).

Conflict of Interest

The authors declare no conflict of interest.

Data Availability Statement

The data that support the findings of this study are available in the Supporting Information of this article.

Keywords: β-Turns · Chiral Resolution · Halogen Bonds · Hydrogen Bonds · Supramolecular Helices

[1] J. Jacques, A. Collet, S. H. Wilen, *Enantiomers, Racemates, and Resolutions*, Krieger, Malabar, **1994**.
[2] L. Pérez-García, D. B. Amabilino, *Chem. Soc. Rev.* **2002**, *31*, 342–356.
[3] L. Pérez-García, D. B. Amabilino, *Chem. Soc. Rev.* **2007**, *36*, 941–967.
[4] A. Gavezzotti, S. Rizzato, *J. Org. Chem.* **2014**, *79*, 4809–4816.
[5] R. K. Hylton, G. J. Tizzard, T. L. Threlfall, A. L. Ellis, S. J. Coles, C. C. Seaton, E. Schulze, H. Lorenz, A. Seidel-

Morgenstern, M. Stein, S. L. Price, *J. Am. Chem. Soc.* **2015**, *137*, 11095–11104.
[6] L.-C. Sögütoglu, R. R. E. Steendam, H. Meekes, E. Vlieg, F. P. J. T. Rutjes, *Chem. Soc. Rev.* **2015**, *44*, 6723–6732.
[7] M. Liu, L. Zhang, T. Wang, *Chem. Rev.* **2015**, *115*, 7304–7397.
[8] E. Yashima, N. Ousaka, D. Taura, K. Shimomura, T. Ikai, K. Maeda, *Chem. Rev.* **2016**, *116*, 13752–13990.
[9] X. Yan, Q. Wang, X. Chen, Y.-B. Jiang, *Adv. Mater.* **2020**, *32*, 1905667.
[10] H. Jędrzejewska, A. Szumna, *Chem. Rev.* **2017**, *117*, 4863–4899.
[11] T. B. Norsten, R. McDonald, N. R. Branda, *Chem. Commun.* **1999**, 719–720.
[12] I. Azumaya, D. Uchida, T. Kato, A. Yokoyama, A. Tanatani, H. Takayanagi, T. Yokozawa, *Angew. Chem. Int. Ed.* **2004**, *43*, 1360–1363; *Angew. Chem.* **2004**, *116*, 1384–1387.
[13] G.-C. Ou, L. Jiang, X.-L. Feng, T.-B. Lu, *Inorg. Chem.* **2008**, *47*, 2710–2718.
[14] Y.-Q. Lan, S.-L. Li, Z.-M. Su, K.-Z. Shao, J.-F. Ma, X.-L. Wang, E.-B. Wang, *Chem. Commun.* **2008**, 58–60.
[15] Q. Gao, F.-L. Jiang, M.-Y. Wu, Y.-G. Huang, D.-Q. Yuan, W. Wei, M.-C. Hong, *CrystEngComm* **2009**, *11*, 918–926.
[16] H. Zhao, W. Q. Ong, F. Zhou, X. Fang, X. Chen, S. F. Y. Li, H. Su, N.-J. Cho, H. Zeng, *Chem. Sci.* **2012**, *3*, 2042–2046.
[17] Z. Xu, H. Liu, M. H. R. Mahmood, Y. Cai, X. Xu, Y. Tang, *CrystEngComm* **2014**, *16*, 3839–3842.
[18] G. M. Upadhyay, H. M. Mande, D. K. Pithadia, R. H. Maradiya, A. V. Bedekar, *Cryst. Growth Des.* **2019**, *19*, 5354–5361.
[19] J.-H. Huang, Z.-Y. Wang, S.-Q. Zang, T. C. W. Mak, *ACS Cent. Sci.* **2020**, *6*, 1971–1976.
[20] T. Buhse, J.-M. Cruz, M. E. Noble-Terán, D. Hochberg, J. M. Ribó, J. Crusats, J.-C. Micheau, *Chem. Rev.* **2021**, *121*, 2147–2229.
[21] P. K. Mandal, G. W. Collie, B. Kauffmann, I. Huc, *Angew. Chem. Int. Ed.* **2014**, *53*, 14424–14427; *Angew. Chem.* **2014**, *126*, 14652–14655.
[22] X.-S. Yan, K. Wu, Y. Yuan, Y. Zhan, J.-H. Wang, Z. Li, Y.-B. Jiang, *Chem. Commun.* **2013**, *49*, 8943–8945.
[23] X.-S. Yan, H. Luo, K.-S. Zou, J.-L. Cao, Z. Li, Y.-B. Jiang, *ACS Omega* **2018**, *3*, 4786–4790.
[24] D. Shi, J. Cao, P. Weng, X. Yan, Z. Li, Y.-B. Jiang, *Org. Biomol. Chem.* **2021**, *19*, 6397–6401.
[25] X. Yan, J. Cao, Y. Zhang, P. Weng, D. Miao, Z. Zhao, Z. Li, Y.-B. Jiang, *Chem. Commun.* **2021**, *57*, 1802–1805.
[26] J. Cao, X. Yan, W. He, X. Li, Z. Li, Y. Mo, M. Liu, Y.-B. Jiang, *J. Am. Chem. Soc.* **2017**, *139*, 6605–6610.
[27] X. Yan, K. Zou, J. Cao, X. Li, Z. Zhao, Z. Li, A. Wu, W. Liang, Y. Mo, Y. Jiang, *Nat. Commun.* **2019**, *10*, 3610.
[28] X. Yan, P. Weng, D. Shi, Y.-B. Jiang, *Chem. Commun.* **2021**, *57*, 12562–12574.
[29] P. Weng, X. Yan, J. Cao, Z. Li, Y.-B. Jiang, *Chem. Commun.* **2022**, *58*, 6461–6464.
[30] T. Tian, R. Hu, B. Z. Tang, *J. Am. Chem. Soc.* **2018**, *140*, 6156–6163.
[31] V. Vasylyeva, S. K. Nayak, G. Terraneo, G. Cavallo, P. Metrangolo, G. Resnati, *CrystEngComm* **2014**, *16*, 8102–8105.
[32] Deposition Numbers 2077476 (for L-**AcAI**), 2077477 (for D-**AcAI**), 2077474 (for L-**AcABr**), 2077475 (for D-**AcABr**), 2077472 (for L-**AcACl**), 2077473 (for D-**AcACl**), 2077469 (for L-**AcAF**), 2077470 (for D-**AcAF**), 2077471 (for *rac*-**AcAF**), 2077467 (for D-**AcAH**), and 2077468 (for *rac*-**AcAH**) contains the supplementary crystallographic data for this paper. These data are provided free of charge by the joint Cambridge Crystallographic Data Centre and Fachinformationszentrum Karlsruhe Access Structures service.

Manuscript received: April 22, 2022
Accepted manuscript online: May 30, 2022
Version of record online: July 12, 2022